Design of a Novel Miniaturized Implantable PIFA for Biomedical Telemetry

A. Kiourti (1), M. Christopoulou (1), S. Koulouridis (2) and K.S. Nikita (1)

(1) National Technical University of Athens, School of Electrical & Computer Engineering
(2) University of Patras, Department of Electrical & Computer Engineering
{akiourti,mchrist}@biosim.ntua.gr;
koulouridis@ece.upatras.gr; knikita@cc.ece.ntua.gr

Abstract. A broadband, circular, double-stacked, implantable planar inverted-F antenna (PIFA) is proposed for biomedical telemetry at f_0= 402 MHz. Both patches are meandered and a high permittivity substrate material is used to limit the radius and height of the antenna to 3.6 mm and 0.7 mm, respectively. The tuning and radiation characteristics as well as the specific absorption rate (SAR) distribution induced by the proposed antenna implanted inside a skin-tissue simulating box and inside the skin layer of a three-layer spherical human head model are evaluated. Finite-difference time-domain (FDTD) simulations are performed and validated through finite-element-method (FEM) simulations. The feasibility of the communication link between the proposed antenna implanted in the spherical head model and an exterior $\lambda_0/2$ dipole antenna is also examined.

Keywords. Biomedical telemetry, implantable antenna, meanders, planar inverted-F antenna (PIFA), shorting pin, specific absorption rate (SAR).

1. Introduction

Recently, biomedical telemetry between antennas implanted inside the human body and exterior equipment has drawn great attention for both medical diagnosis and therapy [1], [2]. In the most common scenario, the signals are wirelessly transmitted at the medical implant communication service (MICS) band of 402 – 405 MHz, which is allocated for ultra-low-power active medical implants [3]. Miniaturization and biocompatibility of the antenna, bandwidth broadening to avoid frequency shift effects and optimization of the radiation performance are the main design constraints of the antenna [4], [5]. Furthermore, regulating the power delivered to the antenna to satisfy the specific absorption rate (SAR) limitations [6], [7] in the surrounding tissue in order to ensure patient safety is a critical issue.

In this paper, a novel circular, stacked planar inverted-F antenna (PIFA) is initially designed to be implanted inside a skin-tissue simulating box and operate at f_0= 402 MHz, with a broad bandwidth of 59 MHz. The proposed antenna is subsequently implanted inside the skin-layer of a three-layer spherical human head model. The resonance characteristics and radiation pattern of the antenna, as well as the required input power to satisfy the IEEE C95.1-1999 [6] and IEEE C95.1-2005 [7]

SAR basic restrictions are evaluated in both scenarios. Finally, the performance of the communication link between the antenna implanted in the spherical head model and an exterior $\lambda_0/2$ dipole receiver is examined. The size of the proposed antenna (radius of 3.6 mm, height of 0.7 mm) is reduced compared to any previous related work [4], [5], [8]-[12]. All simulations have been performed using the finite-difference time-domain (FDTD) numerical technique and validated through finite-element-method (FEM) simulations [13].

The paper is organized as follows. In Section 2, the design of the proposed antenna is illustrated. In Section 3, simulation results of the antenna implanted inside a skin-tissue simulating box as well as inside the skin-layer of a three-layer spherical human head model are presented. In Section 4, the performance of the communication link between the proposed antenna implanted in the spherical head model and an exterior $\lambda_0/2$ dipole antenna is evaluated. The paper concludes in Section 5.

2. Antenna Design

The geometry of the proposed antenna is shown in Fig. 1(a)-(d). The antenna consists of a circular ground plane (R_1= 3.6 mm) and two vertically-stacked, circular, meandered patches (R_2= 3.5 mm) used as the radiating elements. Meandering and stacking of the patches increase the length of the current flow and reduce the size of the antenna [14]. Each of the radiating patches is printed on an 0.3 mm-thick Roger 3210 substrate (ε_r=10.2). To ensure biocompatibility and robustness of the antenna, an 0.1 mm-thick Roger 3210 superstrate layer covers the structure [5]. Both radiating patches are fed by means of a 50 Ohm coaxial cable with an inner radius of 0.2 mm (placed at d_f= 2.9 mm from the centre of the ground plane), while a shorting pin with a radius of 0.2 mm connects the ground plane with the lower patch to achieve a further reduction in size (placed at d_s= 3 mm from the centre of the ground plane) [15]. The meander lengths of the lower patch are given in Table 1. The meander numbers start at the top (feed point location) and increase in number to the bottom (shorting pin location) of the patch. The width of the meanders equals 0.5 mm. The upper patch is an inverted version of the lower patch.

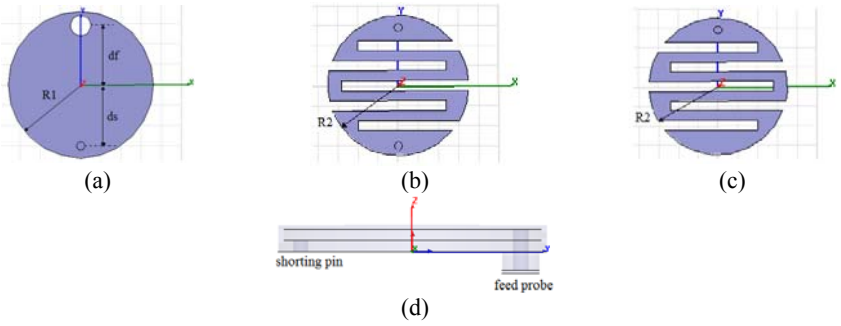

(a) (b) (c)

(d)

Fig. 1. Geometry of the proposed implantable antenna: (a) ground plane, (b) lower patch, (c) upper patch and (d) side view.

Table 1. Meander lengths of the lower patch.

Meander	Length (mm)
1	5.03
2	5.82
3	6.29
4	5.82
5	5.03

The dimensions of the proposed antenna relatively to those of previously reported implantable PIFAs operating at the biomedical frequency band of $402-405$ MHz band are compared in Table 2.

Table 2. Antennas' dimensions comparison.

Antenna	Volume (mm^3)
[4]	$24\times32\times4=3072$
[8]	$20\times24\times2.5=1200$
[9]	$18\times22.5\times1.9=769.5$
[5]	$\pi\times7.5^2\times3\approx530.14$
[10]	$10\times10\times1.905=190.5$
[11]	$\pi\times5^2\times1.815\approx142.55$
[12]	$8\times8\times1.905=121.92$
Proposed	$\pi\times3.6^2\times0.7\approx28.50$

3. Antenna Implanted in Skin-Tissue

Two skin-tissue implantation scenarios are examined for the proposed antenna. The antenna is initially designed and simulated while implanted at the center of an 100 mm-edge cubic box filled with skin-tissue simulating material, as shown in Fig. 2(a). The antenna is subsequently simulated while implanted inside the skin-layer of a three-layer spherical human head model consisting of skin, skull and brain (grey matter) tissues, as shown in Fig. 2(b) [16]. The spherical head model has a radius of 10 cm, while the thicknesses of the skin and skull layers are assumed to be equal to 0.5 cm. Table 3 summarizes the dielectric properties of the tissues used for the simulations at 402 MHz [17]. Free space is assumed for the exterior of the skin-tissue simulating box and the sphere, respectively.

Table 3. Electric properties of the tissues used in the simulations at 402 MHz.

Tissue	Permittivity (ε_r)	Conductivity (σ, S/m)
Skin (dry)	46.7	0.69
Bone (cortical/skull)	13.1	0.09
Brain (grey matter)	57.4	0.74

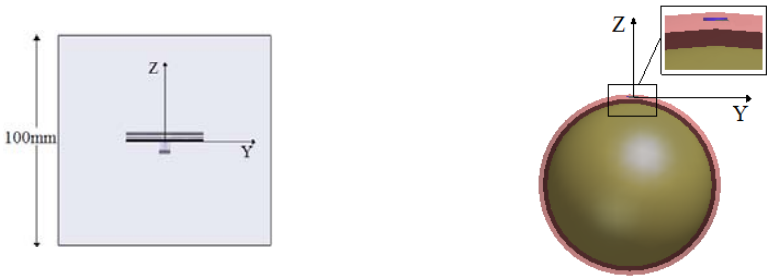

(a) (b)

Fig. 2. Simulation setup of the proposed antenna implanted (a) inside a skin-tissue simulating box and (b) inside the skin-layer of a three-layer spherical human head model.

3.1 Antenna Performance

Assuming that the dielectric properties of the tissues vary negligibly with frequency (inside a small frequency range), the return loss frequency response of the antenna in the scenario of Fig. 2(a) is presented in Fig. 3(a). The antenna resonates at 402 MHz and provides a wide bandwidth of 59 MHz at a return loss less than −10 dB, covering the MICS band under interest. The far-field gain radiation pattern at 402 MHz is shown in Fig. 3(b). Since the antenna is electrically very small, it radiates an omni-directional, monopole-like radiation pattern [18].

The return loss frequency response of the antenna in the scenario of Fig. 2(b) is illustrated in Fig. 4(a). Because of the load effect of the surrounding tissues and the exterior air, the antenna resonant frequency is shifted to 412 MHz and its bandwidth is slightly reduced to 50 MHz at a return loss less than −10 dB. The far-field gain radiation pattern at 402 MHz is slightly modified, but remains omni-directional, as shown in Fig. 4(b).

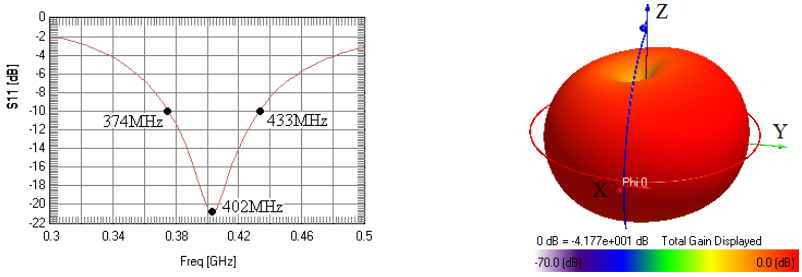

(a) (b)

Fig. 3. (a) Return loss frequency characteristic and (b) Far-field gain radiation pattern at 402 MHz, for the simulation setup of Fig. 2(a).

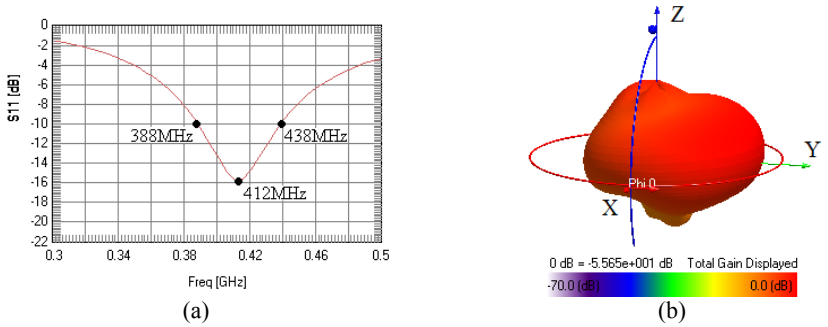

(a) (b)

Fig. 4. (a) Return loss frequency characteristic and (b) Far-field gain radiation pattern at 402 MHz, for the simulation setup of Fig. 2(b).

3.2 SAR Basic Restrictions

In order to assess the electromagnetic power absorbed by the surrounding tissues, an SAR numerical analysis is performed at 402 MHz for the simulation setups of Fig. 2(a) and 2(b). Given that the mass density of the skin, bone and grey matter is equal to 1100 kg/m^3, 1200 kg/m^3 and 1050 kg/m^3, respectively, and assuming that the incident power to the antenna is set to 1 W, the peak 1-g averaged and 10-g averaged SAR values [19] for both scenarios are indicated in Table 4.

In order to satisfy the IEEE C95.1-1999 (1-g averaged SAR < 1.6 W/kg [6]) and IEEE C95.1-2005 (10-g averaged SAR < 2 W/kg [7]) basic restrictions for general public exposure, the power incident to the antenna should not exceed the values of Table 5. Since the peak averaged SAR values for both scenarios were found to be comparable, the maximum allowed power levels for both scenarios are also comparable. Moreover, the IEEE C95.1-1999 standard is found to be stricter, limiting the maximum allowed incident power to the antenna to a value more than ten times lower than that imposed by the IEEE C95.1-2005 standard.

Table 4. Peak 1-g averaged and peak 10-g averaged SAR values for the simulation setups of Fig 2(a) and 2(b) (inc. power 1 W).

Scenario	peak 1-g avg SAR	peak 10-g avg SAR
skin-tissue simulating box	747.7 W/kg	79.76 W/kg
3-layer spherical human head model	739.3 W/kg	76.94 W/kg

Table 5. Maximum allowed incident power to the antenna in the simulation setups of Fig. 2(a) and 2(b) to conform with the IEEE C95.1-1999 and IEEE C95.1-2005 standards.

Scenario	IEEE C95.1-1999	IEEE C95.1-2005
skin-tissue simulating box	< 2.139 mW	< 25 mW
3-layer spherical human head model	< 2.164 mW	< 25.9 mW

3.3 SAR Distribution

In order to satisfy the strictest limitations set by the IEEE guidelines and be able to compare the SAR numerical results for both scenarios, the power incident to the antenna of Fig. 2(a) and 2(b) is assumed to equal 2.139 mW. Local SAR distributions are presented in Fig. 5 and 6 for the two scenarios, respectively, for the slices where maximum local SAR value has been calculated. For comparison reasons, all SAR results have been normalized to 2 W/kg.

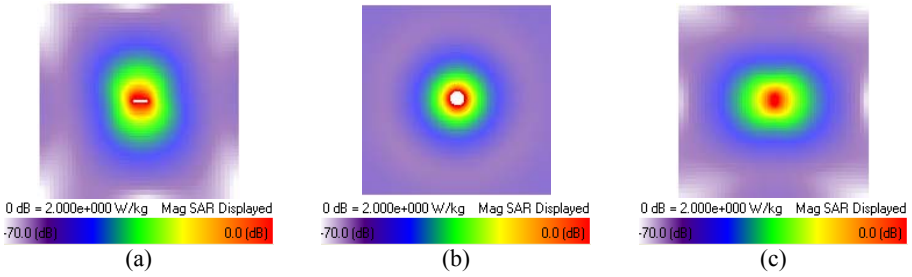

(a) (b) (c)

Fig. 5. Local SAR distribution on the (a) yz, (b) xy and (c) xz slices of the simulation setup of Fig. 2(a) where maximum local SAR has been calculated (inc. power 2.139 mW).

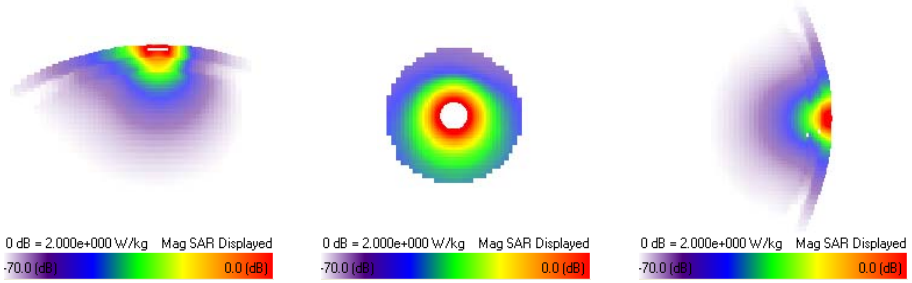

(a) (b) (c)

Fig. 6. Local SAR distribution on the (a) yz, (b) xy and (c) xz slices of the simulation setup of Fig. 2(b) where maximum local SAR has been calculated (inc. power 2.139 mW).

4. Characterization of the Communication Link

Implanted medical devices need a communication link with an exterior monitoring/control unit. In order to characterize the performance of the communication between the proposed antenna when implanted in the spherical head model (transmitter, Tx) and an exterior antenna (receiver, Rx), the simulation setup of Fig. 7(a) is considered. The origin of the coordinate system is located at the center of the implanted antenna's ground plane. A half-wavelength ($\lambda_0/2 \approx 373.14$ mm at $f_0 = 402$ MHz) dipole antenna is placed horizontally above the implanted antenna and

symmetrically around the z axis, so that the centers of the Tx and Rx antennas are aligned. A communication link is built between Tx and Rx.

By moving the exterior dipole antenna along the z axis, or equivalently by changing the distance between the implanted and the exterior antenna, the coupling from Tx to Rx is calculated in terms of the coupling coefficient $|S_{21}|$. The S-parameter $|S_{21}|$ quantifies the power transmission in the wireless link, so that $|S_{21}|^2=P_r/P_t$, where P_t is the incident power at the Tx, and P_r is the power delivered to a 50 Ohm load terminating the Rx [20]. As seen in Fig. 7(b), there is a large variation in coupling strength with distance, with the lowest coupling being for a distally placed Rx.

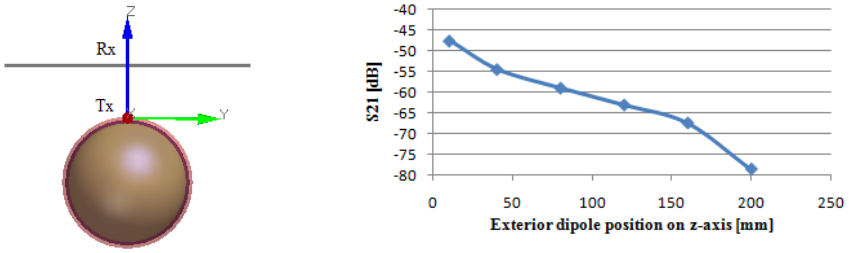

(a) (b)

Fig. 7. (a) Simulation setup for characterizing the communication link. (b) Simulated $|S_{21}|$ versus exterior dipole position on the z-axis.

5. Conclusions

Through studies with the FDTD and FEM electromagnetic solvers, a novel stacked PIFA was designed for skin-tissue implantation and biotelemetry communication at f_0= 402 MHz. The antenna was miniaturized to occupy a volume of 28.5 mm^3 and its tuning and radiation characteristics were evaluated while implanted inside a skin-tissue simulating box as well as inside the skin-layer of a three-layer spherical human head model. The maximum delivered power in both scenarios was estimated such that the SAR values of the surrounding tissues satisfy the IEEE C95.1-1999 and IEEE C95.1-2005 limitations. Finally, the performance of the communication link between the antenna implanted in the spherical head model and an exterior $\lambda_0/2$ dipole antenna was evaluated. The proposed antenna could be integrated in an active medical implant for intracranial pressure (ICP) monitoring [21].

Future work will include numerical calculation of the radiation and SAR characteristics of the proposed antenna while implanted inside an anatomical head model. Subsequent investigations will also include construction of the proposed antenna and experimental validation of the simulation results.

References

1. Weiss M. et al., RF Coupling in a 433-MHz Biotelemetry System for an Artificial Hip, IEEE Antennas & Wireless Prop. Letters, vol. 8, pp. 916-919 (2009)
2. Gosalia K. et al., Thermal Elevation in the Human Eye and Head Due to the Operation of a Retinal Prosthesis, IEEE Trans. Biomed. Eng., vol. 51, no. 8, pp. 1469-1477 (2004)
3. FCC, Medical Implant Communications Service (MICS), (FCC) Std. CFR, Part 95 (1999)
4. Kim J. and Samii Y., Implanted Antennas Inside a Human Body: Simulations, Designs, and Characterizations, IEEE Trans. Micr. Theory & Techn., vol. 52, no.8, pp. 1934-1943 (2004)
5. Rucker D. et al., A Miniaturized Tunable Microstrip Antenna for Wireless Communications with Implanted Medical Devices, Proc. of the ICST 2nd Int. Conf. on BANs (2007)
6. IEEE, Standard for Safety Levels with Respect to Human Exposure to Radio Frequency Electromagnetic Fields, 3kHz to 300GHz (1999)
7. IEEE, Standard for Safety Levels with Respect to Human Exposure to Radio Frequency Electromagnetic Fields, 3kHz to 300GHz (2005)
8. Kim J. and Samii Y., Planar Inverted-F Antennas on Implantable Medical Devices: Meandered Type Versus Spiral Type, Micr. & Opt. Techn. Letters, vol. 48, no.3, pp. 567-572 (2006)
9. Lee C.-M. et al., Bandwidth Enhancement of Planar Inverted-F Antenna for Implantable Biotelemetry, Micr. & Opt. Techn. Letters, vol. 51, no.3, pp. 749-752 (2009)
10. Liu W.-C. et al., Miniaturized Implantable Broadband Antenna for Biotelemetry Communication, Micr.& Opt. Techn. Letters, vol. 50, no. 9, pp. 2407-2409 (2008)
11. Liu W.-C. et al., Implantable Broadband Circular Stacked PIFA Antenna for Biotelemetry Communication, J. of Electromagn. Waves & Appl., vol. 22, pp. 1791-1800 (2008)
12. Liu W.-C. et al., BW Enhancement and Size Reduction of an Implantable PIFA Antenna for Biotelemetry Devices, Micr. & Opt. Techn. Letters, vol. 51, no. 3, pp. 755-757 (2009)
13. Sadiku M., Numerical Techniques in Electromagnetics, CRC Press (2001)
14. Wong K.-L., Compact and Broadband Microstrip Antennas, John Wiley&Sons (2002)
15. Chow Y.L. et al., Miniaturizing Patch Antenna by Adding a Shorting Pin Near the Feed Probe - a Folded Monopole Equivalent, IEEE Ant. & Prop. Symp. vol. 4, pp. 6-9 (2002)
16. Koulouridis S. and Nikita K.S., Study of the Coupling Between Human Head and Cellular Phone Helical Antennas, IEEE Trans. on Electromagn. Compat., vol. 46, no. 1, pp. 62-70 (2004)
17. Gabriel C. et al., The dielectric properties of biological tissues, Phys. Med. Biol., vol. 41, pp. 2231-2293 (1996)
18. Abadia J. et al., 3D-Spiral Small Antenna Design and Realization for Biomedical Telemetry in the MICS Band, Radioengineering, vol. 18, no. 4, pp. 359-367 (2009)
19. IEEE Recommended Practice for Measurements & Computations of RF EM fields with Respect to Human Exposure to Such Fields, IEEE Standard C95.3-2002 (2002)
20. Warty R. et al., Characterization of Implantable Antennas for Intracranial Pressure Monitoring: Reflection by and Transmission Through a Scalp Phantom, IEEE Trans. Micr. Theory & Techn., vol. 56, no. 10, pp. 2366-2376 (2008)
21. Kawoos U. et al., In-Vitro and In-Vivo Trans-Scalp Evaluation of an Intracranial Pressure Implant at 2.4GHz, IEEE Trans. Micr. Theory & Techn., vol. 56, no.10, pp. 2356-2365 (2008)